REPORT DOCUMENTATION PAGE

1. REPORT DATE (DD-MM-YYYY) 09 January 2016	2. REPORT TYPE Technical Paper	3. DATES COVERED (From - To) 24 November 2015 – 09 January 2016

4. TITLE AND SUBTITLE	5a. CONTRACT NUMBER
Investigation of the Stability of POD-Galerkin Techniques for Reduced Order Model Development	
	5b. GRANT NUMBER
	5c. PROGRAM ELEMENT NUMBER

6. AUTHOR(S)	5d. PROJECT NUMBER
Huang, C., Anderson, W., Merkle, C. and Sankaran, V.	
	5e. TASK NUMBER
	5f. WORK UNIT NUMBER Q12J

7. PERFORMING ORGANIZATION NAME(S) AND ADDRESS(ES) AND ADDRESS(ES)	8. PERFORMING ORGANIZATION REPORT NO.
Air Force Research Laboratory (AFMC) AFRL/RQR 5 Pollux Drive Edwards AFB, CA 93524-7048	

9. SPONSORING / MONITORING AGENCY NAME(S) AND ADDRESS(ES)	10. SPONSOR/MONITOR'S ACRONYM(S)
Air Force Research Laboratory (AFMC)	
AFRL/RQR 5 Pollux Drive Edwards AFB, CA 93524-7048	11. SPONSOR/MONITOR'S REPORT NUMBER(S) AFRL-RQ-ED-TP-2015-434

12. DISTRIBUTION / AVAILABILITY STATEMENT
Approved for public release; Distribution Unlimited

13. SUPPLEMENTARY NOTES
For presentation at 2016 AIAA SciTech Meeting; San Diego, CA (04-09 January 2016) PA Clearance Number 15704; Clearance Date 12/15/2015

14. ABSTRACT
Detailed investigations are performed to analyze and mitigate the stability issues encountered in developing a reduced order model (ROM) for combustion response to specified excitations using the Euler equations. The ROM is obtained by employing Galerkin's method to reduce the high-order PDEs to a lower-order ODE system by means of POD eigen-bases. Possible solutions of the ROM stability issues by changing and/or by scaling the equation variables are discussed following suggestions from previous Euler equations studies. However, our evaluations using the linearized Euler equations indicate that spurious unstable modes are still encountered in the resulting ROMs. Different mean flow and boundary conditions are implemented to further evaluate the ROMs, which indicate that the presence of upstream propagating characteristic waves play an important role in affecting ROM stability. Increasing the added artificial dissipation terms is proposed and shown to be an effective method that insures that the ROMs are both numerically stable and capable of accurately reproducing the CFD solutions.

15. SUBJECT TERMS
N/A

16. SECURITY CLASSIFICATION OF:			17. LIMITATION OF ABSTRACT	18. NUMBER OF PAGES	19a. NAME OF RESPONSIBLE PERSON V. Sankaran
a. REPORT Unclassified	b. ABSTRACT Unclassified	c. THIS PAGE Unclassified	SAR	22	19b. TELEPHONE NO (include area code) N/A

Investigation of the Stability of POD-Galerkin Techniques for Reduced Order Model Development

Cheng Huang[*], William E. Anderson[†], Charles L. Merkle[‡]

Purdue University, West Lafayette, IN, 47907

and

Venkateswaran Sankaran[§]

Air Force Research Laboratory (AFRL), Edwards AFB, CA, 93524

Detailed investigations are performed to analyze and mitigate the stability issues encountered in developing a reduced order model (ROM) for combustion response to specified excitations using the Euler equations. The ROM is obtained by employing Galerkin's method to reduce the high-order PDEs to a lower-order ODE system by means of POD eigen-bases. Possible solutions of the ROM stability issues by changing and/or by scaling the equation variables are discussed following suggestions from previous Euler equations studies. However, our evaluations using the linearized Euler equations indicate that spurious unstable modes are still encountered in the resulting ROMs. Different mean flow and boundary conditions are implemented to further evaluate the ROMs, which indicate that the presence of upstream propagating characteristic waves play an important role in affecting ROM stability. Increasing the added artificial dissipation terms is proposed and shown to be an effective method that insures that the ROMs are both numerically stable and capable of accurately reproducing the CFD solutions.

I.   Introduction

Combustion instability is a complex phenomenon that results from the coupling between the modes of heat release and acoustics. In practical combustor devices the complexity is greatly amplified by turbulent, compressible flow, very high rates of heat release, and complicated geometries and acoustic boundary conditions. Modern computational capability offers the potential for moving beyond the empirically-based design analysis of the past,

---

but high-fidelity simulations of full scale dynamics for engineering analysis are still out of reach. However, high fidelity simulations of smaller scale domains can be used to obtain reduced order models of the combustion response that can accurately describe the linear/nonlinear coupling between acoustics and combustion and can subsequently be used to analyze full-scale configurations.

The model reduction techniques have been devised to develop numerically stable and robust reduced order models (ROM) [1-3] and they have been applied to non-reacting flow problems including flow control [4-6] and unsteady aeroelasticity [7, 8]. Recent studies have extended ROMs to combustion problems [9, 10]. A preliminary exploration of the POD/Galerkin technique using a model reaction-advection scalar equation for developing valid reduced-order models was performed by Huang et al. [11], which assessed the capability of the ROM for predicting responses at target frequencies. This work was further extended to establish ROM performance for the Euler system of equations [16].

A major focus of these previous studies focus on identifying and resolving robustness and stability issues associated with the ROM development. As reported, the issues can come from the inherent lack of numerical stability in the POD/Galerkin method itself [12], truncation of low-energy dissipative POD modes [1] and simplifications of higher-order equations [13]. The balanced POD technique has been proposed to build numerically stable ROM for linear systems [2, 14]. Bergmann et al. proposed to add residuals of the Navier-Stokes equations to account for the absence of low-energy dissipative POD modes [1]. Moreover, Lucia et al. [15] demonstrated the effectiveness of constructing stable ROM by including additional artificial dissipation terms. In addition to including artificial terms in building ROM, researchers have also tried to resolve the issues based on the numerical properties of the system equations. Barone et al [17, 18] proposed to stabilize the reduced system by symmetrizing the higher-order PDE with a preconditioning matrix. Rowley et al. also pointed out that defining a proper inner product can be important when dealing with model reduction of the Navier-Stokes equations [3]. For aeroelastic applications, Amsallen and Farhat have shown the advantages of using the descriptor form over non-descriptor form of the governing equations [19].

It is important to point out that the stability issues in the above studies were generally associated with ROMs that were built using a partial or incomplete set of POD modes. Indeed, our previous scalar equation studies have shown that spurious unstable modes can be generated if an incomplete set of POD modes (100% of the energy content) is used to build the ROM [11]. Conversely, it was also shown that, for the scalar equation, using a complete POD set always insured a stable ROM [11]. However, for the vector system of Euler equations, Huang et al. identified that stability issues in the ROM can arise even when a complete set of POD modes is included [16]. Based on the knowledge above, in this paper, the stability issues that arise in the ROM development of the vector system of Euler equations [16] are investigated for possible causes and solutions to avoid spurious unstable modes. Again, we note that the complete set of POD modes is used in this study to build the ROM instead of a partial set as commonly done in reduced order development.

The remainder of the paper is organized as follows. In Section II, we present the Euler equations with a modeled combustion source term and the forcing function and boundary conditions used. In addition, we also present the

2

Galerkin formulation and the POD techniques for deriving reduced order models for the linearized version of the Euler equations. In Section III, a summary is given with regard to previous efforts to build stable ROMs by changing the solution variables used for the POD generation [16]. In Section IV, we describe the test problem and summarize the mean flow conditions used for ROM studies. In Section V, we demonstrate the existence of stability issues and the corresponding consequences in ROM development. We then use different mean flow and boundary conditions to evaluate their effects on ROM stability and draw some conclusions regarding when the stability problems occur. Following this, we propose and test the inclusion of additional artificial dissipation to mitigate the stability issues. In the final section, we provide concluding remarks and suggest future directions for continued research.

II. Formulation

A. Governing equations

The governing equations are the quasi-one-dimensional unsteady Euler equations with a single-step chemical reaction and a specified reaction distribution,

$$\frac{\partial \mathbf{Q}}{\partial t} + \frac{\partial \mathbf{E}}{\partial x} = \mathbf{H} + \mathbf{H}_f + \mathbf{H}_q \tag{1}$$

where,

$$\mathbf{Q} = \begin{pmatrix} \rho A \\ \rho u A \\ e A \\ \rho Y_{ox} A \end{pmatrix}, \quad \mathbf{E} = \begin{pmatrix} \rho u A \\ \left(\rho u^2 + p \right) A \\ \left(e + p \right) A \\ \rho u Y_{ox} A \end{pmatrix}, \quad \mathbf{H} = \begin{pmatrix} 0 \\ p\dfrac{dA}{dx} \\ 0 \\ 0 \end{pmatrix}, \quad \mathbf{H}_f = \begin{pmatrix} \dot{\omega}_f \\ \dot{\omega}_f \bar{u} \\ \dot{\omega}_f \left(\bar{h}_0 - \dfrac{\bar{p}}{\bar{\rho}} \right) \\ -\dot{\omega}_{ox} \end{pmatrix}, \quad \mathbf{H}_q = \begin{pmatrix} 0 \\ 0 \\ \dot{q}''' \\ 0 \end{pmatrix}.$$

Here x and t are the space and time variables, ρ is the density, u is the velocity, e is the total energy, p is the pressure, Y_{ox} is the oxidizer mass fraction and $A = A(x)$ is the cross-section area of the geometry. The effects of fuel addition are accounted through steady source term $\mathbf{H}_f$, where $\dot{\omega}_f = C_{f/O}\dot{\omega}_{ox}$ with constant $C_{f/O}$ representing fuel-to-oxidizer ratio and a sinusoidal spatial distribution is used to model the oxidizer reaction, $\dot{\omega}_{ox} = k_f \bar{\rho} \bar{Y}_{ox} \left(1 + \sin\left(-\dfrac{\pi}{2} + \dfrac{x - l_s}{l_f - l_s} 2\pi \right) \right)$, $(\forall\, l_s < x < l_f)$, where l_s and l_f are the axial locations of the beginning and end of the combustion zone. The reaction constant k_f is selected to ensure that the oxidizer is consumed within the specified combustion zone. The unsteady combustion response is accounted in the source term, $\mathbf{H}_q$, using the n-τ model [20], $\dot{q}''' = \bar{q} \cdot n \cdot \alpha(x) \dfrac{p(x, t - \tau) - \bar{p}(x)}{\bar{p}(x)}$, which relates the unsteady heat release to the pressure oscillations through an index, n and a time lag constant, τ. Here $\bar{q}$ is the integral mean combustion heat release and $\alpha(x)$ is a

scaling function following a normal distribution, $\alpha(x) = \dfrac{1}{\sigma\sqrt{2\pi}}\exp\left(-\dfrac{(x-\mu)^2}{2\sigma^2}\right)$. This model was previously used

[21] to simulate combustion instability in a longitudinal rocket combustor,

For simplicity, the linearized version of Eq. (1) is used for the studies in ROM development,

$$\overline{\Gamma}_p \frac{\partial \mathbf{Q}'_p}{\partial t} + \frac{\partial \overline{A}_p \mathbf{Q}'_p}{\partial x} = \overline{D}_p \mathbf{Q}'_p \tag{2},$$

where $\mathbf{Q}'_p = \left(p' \quad u' \quad T' \quad Y'_{ox} \right)^{\mathrm{T}}$, $\overline{\Gamma}_p = \left.\dfrac{\partial \mathbf{Q}}{\partial \mathbf{Q}_p}\right|_{\overline{\mathbf{Q}}_p}$, $\overline{A}_p = \left.\dfrac{\partial \mathbf{E}}{\partial \mathbf{Q}_p}\right|_{\overline{\mathbf{Q}}_p}$ and $\overline{D}_p = \left.\left(\dfrac{\partial \mathbf{H}}{\partial \mathbf{Q}_p} + \dfrac{\partial \mathbf{H}_q}{\partial \mathbf{Q}_p}\right)\right|_{\overline{\mathbf{Q}}_p}$.

B. Boundary conditions

Fluctuating conditions inside the computational domain are obtained by specifying periodic oscillations of target quantities ($\phi'(t)$), which can be mass flow rate ($\dot{m}'(t)$), back pressure (p'_{back}) or the Riemann variables, about their mean value (ϕ_0),

$$\phi'(t) = \phi_0 \frac{\varepsilon}{N_f} \sum_{k=1}^{N_f} \sin\left(2\pi\left(f_0 + \Delta f\right)t\right) \tag{3},$$

where f_0 is the initial frequency; Δf represents the fundamental frequency increment and N_f is the total number of frequencies included in the forcing function. The fundamental period T_p is determined by Δf such that $T_p = 1/\Delta f$. Note that if $\Delta f = f_0$, Eq. (3) represents a standard Fourier series although herein we generally take $\Delta f < f_0$ so that Eq. (3) differs from a Fourier series.

Four different boundary conditions (summarized in Table 1) are implemented to help further understand and identify the causes of numerical stability issues arising from the previous ROM study for the Euler equations [16].

	B.C. label	Upstream	Downstream
Subsonic flow	1	$\dot{m}$, T^0 and Y_{ox}	p_{back}
	2	Riemann invariant B.C.	Non-reflecting
	3	$\dot{m}$, T^0 and Y_{ox}	Non-reflecting
Supersonic flow	4	p^0, $\dot{m}$, T^0 and Y_{ox}	/

Table 1 Summary of boundary conditions.

C. Construction of POD eigen-bases for vector equations

POD eigen-bases are calculated based on the CFD solutions, $\mathbf{Q}'_p(x,t)$ obtained from Eq. (2) using the vector-valued method,

$$P(x)\mathbf{Q}'_p(x,t) \approx \sum_{n=1}^{N_p} \hat{a}_n(t)\sigma_n\mathbf{\Phi}_n(x) = \sum_{n=1}^{N_p} \hat{a}_n(t)\sigma_n \begin{pmatrix} \phi_{p,n}(x) \\ \phi_{u,n}(x) \\ \phi_{T,n}(x) \\ \phi_{Y_{ox},n}(x) \end{pmatrix} = \sum_{n=1}^{N_p} a_n(t) \begin{pmatrix} \phi_{p,n}(x) \\ \phi_{u,n}(x) \\ \phi_{T,n}(x) \\ \phi_{Y_{ox},n}(x) \end{pmatrix} \quad (4),$$

where σ_n is the singular value of the nth POD mode (scalar), $a_n(t)$ is the nth POD temporal mode (scalar), and the nth eigen-mode, $\mathbf{\Phi}_n(x)$, is an orthonormal vector function,

$$\int_X \mathbf{\Phi}_n^{\text{T}}(x)\mathbf{\Phi}_n(x)dx = \begin{cases} 1, & \text{if } k = n \\ 0, & \text{otherwise} \end{cases}, \quad X = \{0 \le x \le L\} \quad (5).$$

It should be noted that, unlike in the scalar equation case, to obtain reasonably scaled POD eigen-bases for the vector variables, a normalization matrix $P(x)$ must be used before calculating the POD eigen-bases. Likewise, to reconstruct the CFD solutions using the POD eigen-bases, the matrix $P(x)$ again needs to be included,

$$\mathbf{Q}'_p(x,t) \approx P^{-1}(x)\sum_{n=1}^{N_p} a_n(t) \begin{pmatrix} \phi_{p,n}(x) \\ \phi_{u,n}(x) \\ \phi_{T,n}(x) \\ \phi_{Y_{ox},n}(x) \end{pmatrix} \quad (6).$$

Different definitions of P(x) are given later.

D. Model reduction of Euler equations

The application of the POD-Galerkin method to the linearized Euler equations (Eq. (2)) is briefly introduced here. Additional details can be found in Ref [11]. Upon obtaining the eigen-bases as in Eq. (4), the target governing equation is projected onto the kth eigen-mode, $\mathbf{\Phi}_k(x)$, throughout the whole computational domain. Before the projection the governing equation needs to be normalized by pre-multiplying by the matrix $P(x)$,

$$\int_X \mathbf{\Phi}_k^{\text{T}}(x)P(x)\left(\frac{\partial \mathbf{Q}'_p(x,t)}{\partial t} + \bar{\Gamma}_p^{-1}(x)\frac{\partial \bar{A}_p(x)\mathbf{Q}'_p(x,t)}{\partial x}\right)dx = \int_X \mathbf{\Phi}_k^{\text{T}}(x)P(x)\bar{\Gamma}_p^{-1}(x)\bar{D}_p(x)\mathbf{Q}'_p(x,t)dx \quad (7),$$

Substituting the POD expansion, Eq. (6) into Eq. (7) and using a numerical quadrature to approximate the integrals,

$$\sum_{n=1}^{N_p} \left\{ \sum_{i=1}^{NI} \mathbf{\Phi}_{k,i}^{\mathrm{T}} P_i P_i^{-1} \mathbf{\Phi}_{n,i} \Delta x_i \right\} \dot{a}_n(t)$$

$$+ \sum_{n=1}^{N_p} \left\{ \sum_{i=1}^{NI} \left(\mathbf{\Phi}_{k,i}^{\mathrm{T}} P_i \overline{\Gamma}_{p,i}^{-1} \left(\frac{\delta \overline{A}_p P^{-1} \mathbf{\Phi}_n}{\delta x} \right)_i - \mathbf{\Phi}_{k,i}^{\mathrm{T}} P_i \overline{\Gamma}_{p,i}^{-1} \overline{D}_{p,i} P_i^{-1} \mathbf{\Phi}_{n,i} \right) \Delta x_i \right\} a_n(t) = 0 \tag{8}.$$

Following the model reduction procedure in Ref [11] and using a consistent discretization scheme (a 2nd-order upwind scheme is used in both CFD and ROM) to approximate the gradient term in Eq. (8), an ODE system can be obtained with the contributions from boundary conditions appearing as a source term on the right-hand-side,

$$\frac{d\mathbf{a}(t)}{dt} - L\mathbf{a}(t) = \mathbf{h}(t) \tag{9},$$

where $\mathbf{a}(t) = \begin{bmatrix} a_1(t) & \cdots & a_k(t) & \cdots & a_{N_p}(t) \end{bmatrix}^{\mathrm{T}}$,

$\mathbf{h}(t) = \begin{bmatrix} h_1(t) & \cdots & h_k(t) & \cdots & h_{N_p}(t) \end{bmatrix}^{\mathrm{T}}$ with contributions from boundary conditions, $h_k(t) = F_k(\phi'(t))$,

L is the stiffness matrix which describes the dynamics of the reduced ODE system.

III. Background

Our previous studies with the scalar equation have demonstrated that using a complete set of POD modes is sufficient to insure stability in the ROM development [11]. However, perhaps surprisingly, our studies with the vector system of Euler equations indicate that this is no longer the case [16]. In other words, spurious unstable modes are encountered even when the ROM Is developed using the complete set of POD modes. In fact, this problem arises even for the simple problem of acoustic modes in a straight duct without combustion, which should be stable by definition. It has also been demonstrated in our previous study that different scaling strategies of the solution variables can be helpful in getting rid of the spurious unstable modes [16]. Moreover, as mentioned in the introduction, it has been reported by other researchers that an appropriate treatment of solution variable for the POD mode calculation can be useful in resolving the ROM stability issues. Therefore, the effects of different solution variable treatments on the ROM stability are briefly discussed in this section.

First, the scaling of temperature fluctuations (T') is tuned through parameter, α, by defining the matrix $P(x)$ in Eq. (4) as,

$$P(x) = \mathrm{diag}\left(1/p'_{\max}, 1/u'_{\max}, \alpha/T'_{\max}, 1/Y'_{ox,\max}\right) \tag{10},$$

where $p'_{\max} = \mathrm{Max}\{p'(x,t)\}$, $\forall \ 0 \le x \le L$ and t so that the variations in each variable can be taken into account in relative to their maximum amplitude. As an example, CFD solutions are generated using B.C. 1 in Table 1 by perturbing the inlet mass flow. Two specific forcing functions are considered with 3 and 5 frequencies included. As

in the previous studies [16], the eigen-values of stiffness matrix L in Eq. (9) are investigated to assess the numerical stability of the resulting ROMs. The real parts (σ) of the eigen-values are plotted against the scaling parameter, α, for the two forcing functions in Fig. 1. It is noted that a stable ROM ($\sigma < 0$) can be achieved for an appropriate value of the scaling parameter. However, the two cases shown here do not share a common scaling strategy that insures stability in both ROMs, which means that the choice of scaling is problem-dependent.
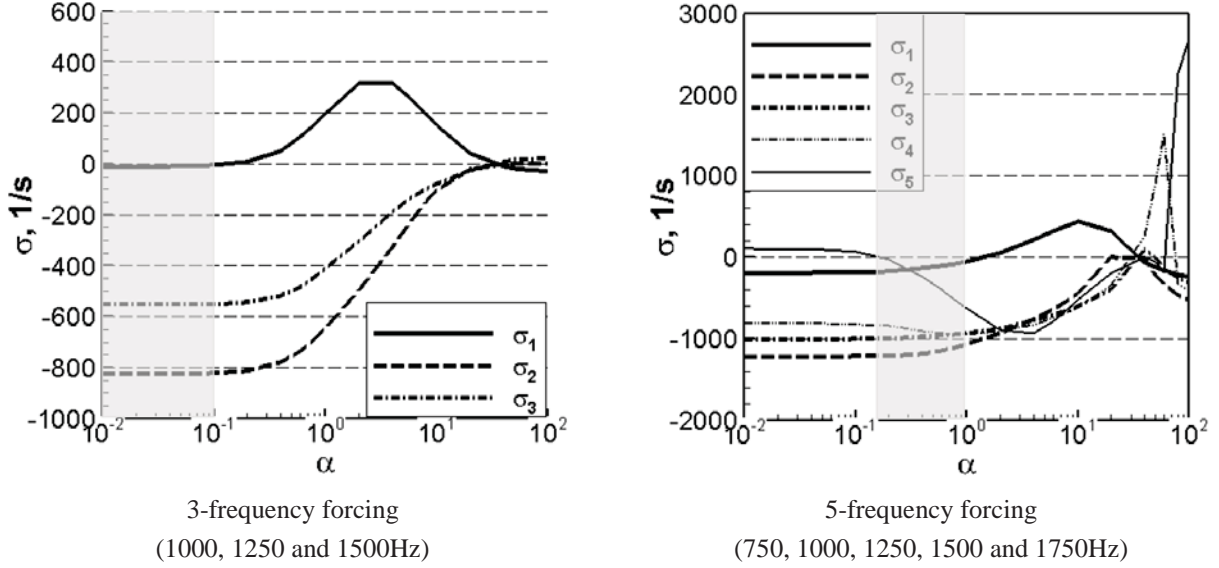

3-frequency forcing
(1000, 1250 and 1500Hz)

5-frequency forcing
(750, 1000, 1250, 1500 and 1750Hz)

Figure 1 The scaling effects on the eigen-values of resulting ROMs using p', u', T' and Y'_{ox} as solution variables (the stable region, $\sigma < 0$, is covered by the grey box).

As a second example, different solution variables (summarized in Table 2) from the same CFD simulation are selected to build the ROM. The CFD solutions are generated using the 3-frequency forcing. The set 1 in Table 2 uses the same solution variables (p', u', T' and Y'_{ox}) as in Fig. 1 and all variables are scaled to the same fluctuating levels ($\alpha = 1$ in Eq. (10)). Set 2 uses the same scaling strategy as set 1 but instead of using temperature fluctuations (T'), density (ρ') is used. Set 3 follows the strategy derived by Barone et al. [17]. Their method symmetrizes the governing equations by pre-multiplying a matrix S and choose the solution variables as

$$\mathbf{Q}'_S = \left(u' \quad (1/\rho)' \quad p' \quad Y'_{ox} \right)^{\mathrm{T}},$$

$$S = \begin{pmatrix} \overline{\rho} & 0 & 0 & 0 \\ 0 & \gamma\overline{p}\overline{\rho}^2 & \overline{\rho} & 0 \\ 0 & \overline{\rho} & \dfrac{2}{\gamma\overline{p}} & 0 \\ 0 & 0 & 0 & \gamma\overline{p} \end{pmatrix} \tag{11},$$

where γ is the ratio of the constant volume and constant pressure heat capacity. And then the POD modes, $\mathbf{\Phi}_k$, are

calculated based upon the transformed variables $\mathbf{Q}'_T = S^{1/2}\mathbf{Q}'_S \approx \sum\limits_{k=1}^{N_p} a_k(t)\mathbf{\Phi}_k(x)$.

Case Name	Variables
Set 1	p', u', T' and Y'_{ox}
Set 2	p', u', ρ' and Y'_{ox}
Set 3	Symmetrizing variables [17]

Table 2 Summary of solution variables used for ROM construction.

The ROM spectrum comparisons are shown in Fig. 2 for the three solution variables. The real (σ) and imaginary ($2\pi f$) parts of the stiffness matrix L eigen-values are plotted against each other. Unstable eigen-modes ($\sigma > 0$, highlighted using dashed circle) can be seen using solution variables set 1 and 3 while a stable ROM can be obtained using set 2 variables. On the other hand, when different forcing functions are used, we find that ROM stability cannot be guaranteed even for set 2. Moreover, the symmetrizing variables in set 3, which was reported to be capable of generating stable ROMs, also seem to have stability issues here. In addition, we have also tried the conservative set of variables (ρ', $(\rho u)'$, $(\rho h^0 - p)'$ and $(\rho Y_{ox})'$) following Amsallen and Farhat's studies [19] but again, we find that ROM stability cannot be universally guaranteed.
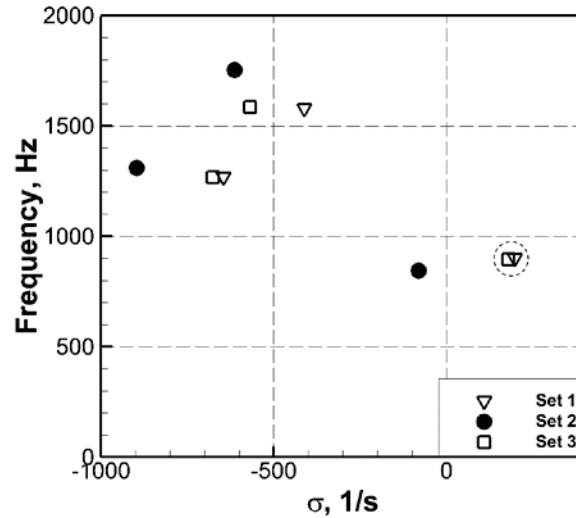

Figure 2 The ROM spectra comparisons for different selections of solution variables for the 3-frequency forcing case (1000, 1250 and 1500Hz).

In summary, the ways to generate POD modes, in terms of either scaling of vector variables or the selection of solution variables can be important in affecting the stability properties of resulting ROMs. However, it seems to be a difficult task to look for a universally valid method for POD mode calculation to resolve the ROM stability issues. Therefore, a further systematic investigation is needed to provide insights regarding possible solutions of the stability issues in reduced order model development.

IV. Overview of Test Problem

A constant-area duct is set up for the ROM development as shown in Fig. 3 with different boundary conditions summarized in Table 1. For a typical computation, the steady state numerical solution of Eq. (1) is computed first. The upstream boundary condition is then switched to a temporally varying periodic condition as defined in Eq. (3) and the time-accurate computation is continued until stationary conditions are reached.

$x/L = 0$ _____ $x/L = 1$

Upstream   Downstream
B.C.   B.C.

Figure 3 Computational setup for the one-dimensional Euler equations.

The solutions are tabulated and stored periodically (i.e., at several time-levels within a forcing period) thereby generating a rectangular matrix that can be used as a database for fitting eigen-bases by means of the POD procedure in Eq. (4). The POD eigen-bases are then applied to the governing linear or nonlinear PDE to derive the reduced-order ODE formulation (or ROM). In order to focus our attention on understanding the numerical stability issues identified in Ref [16], no combustion is included in Eq. (1) and (2) and only gas dynamics (p', u' and T') are solved in the constant-area duct. The five mean flow conditions simulated correspond to a range of Mach numbers summarized in Table 3.

	Case #	Ma	Pressure, MPa	Temperature, K
	A	0.21	1	2000
Subsonic	B	0.46	1	1900
	C	0.86	1	1670
Supersonic	D	1.87	4	2000
	E	2.80	1.5	2000

Table 3 Summary of mean flow conditions.

V. Results

A. Baseline ROM Characteristics

Case A in Table 3 is selected as the baseline for ROM characteristics studies using B.C. 1 in Table 1. It has been reported in previous work that the ROM stability can vary by applying different forcing functions in obtaining CFD solutions using the same boundary conditions [16]. Therefore, six forcing functions, from single to multiple frequencies, are used for ROM generation and are summarized in Table 4. The POD eigen-basis is generated using the vector-valued method defined in Eq. (4) and the three variables (u', p', and T') are normalized by the maximum values of the respective fluctuating quantity throughout the whole domain (i.e. $P(x) = \text{diag}\left(1/p'_{\max}, 1/u'_{\max}, 1/T'_{\max}\right)$ where $p'_{\max} = \text{Max}\left\{p'(x,t)\right\}$, $\forall\ 0 \le x \le L$ and t etc.). Following the conclusion from scalar Equation studies [11], all the meaningful (or non-zero amplitude) POD eigen-bases are used to generate the ROM corresponding in each of the six cases.

Case Name	f_0, Hz	Δf, Hz	# of forcing frequencies	# of necessary POD modes
Singe-frequency		--	1	2
2-frequency		250	2	4
3-frequency	1000	250	3	6
4-frequency		250	4	8
10-frequency		250	10	18
21-frequency		250	21	18

Table 4 Summary of cases used in studies of ROM characteristics for Case A in Table 3.

The eigen-value spectra of the ROM stiffness matrix (L in Eq. (9)) are investigated and shown in Fig. 4 for the six cases in Table 4. For the single-, 2- and 3-frequency forcing cases, all eigen-values are observed to have negative real parts (σ), which indicates that the corresponding ROMs will be stable. Solving the ROM equation for these three cases using the same forcing as used in the CFD solution gives reconstructed solutions that are indeed in excellent agreement with the CFD results as shown in Fig. 5 (top). The ROMs are able to reproduce the original CFD solutions and show no evidence of unphysical or unstable behavior.
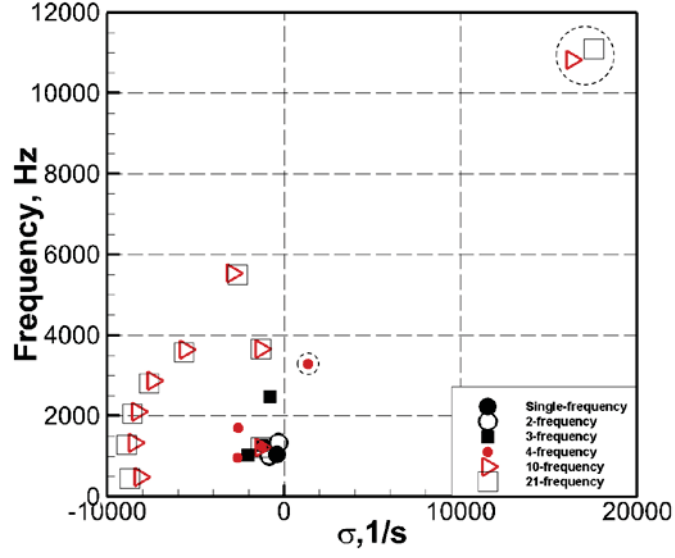
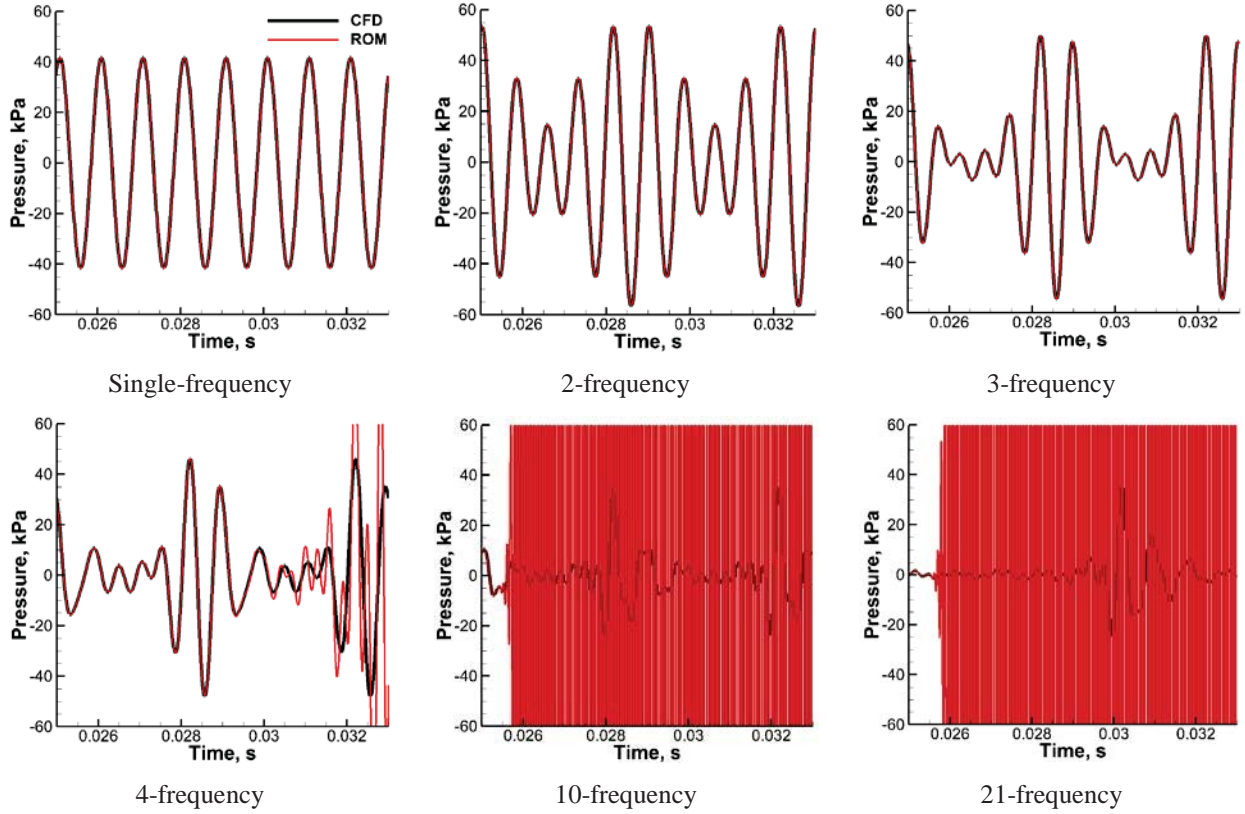**Figure 4 Eigen-value spectrum of ROM stiffness matrix for Case A in Table 3.**

Figure 5 ROM and CFD solutions comparison of Case A at x/L = 0.5 for cases in Table 4.

The remaining three cases with multiple frequencies in the forcing function appear to be more problematic for building stable ROMs. Unstable modes can be observed in the 4-, 10- and 21-frequency cases (highlighted by the dashed circle in Fig. 4) even though a complete set of POD modes have been included in building the ROM. These unstable modes leads to unphysical growth in the ROM solution as shown in Fig. 5 (bottom). With higher growth rate of the unstable eigenvalue, the ROM prediction is seen to go off track faster. In fact, our results suggest that the more diverse the frequencies are in the forcing function, the more difficulties the ROM construction can encounter.

B. Potential causes for stability issues in ROM

To further understand and identify the potential causes for the unstable modes in the ROMs observed in Fig. 5, two major aspects are investigated in this section:

1. So far, the studies have focused on low Mach number flows (Ma < 0.3); so, we study the effects of flow conditions---specifically the Mach number variation---on the ROM stability characteristics. Importantly, we consider the difference between subsonic flow that have characteristic waves traveling in both directions and supersonic flow where the waves are all traveling downstream. Importantly, we note that the latter case more closely resembles the scalar wave equation case.

2. Based on the knowledge from previous studies [11], we know that the stability issues do not arise in the scalar equation studies as long as a complete set of POD modes are included in the ROM construction. We therefore seek to isolate the characteristic waves contained in the Euler equations through control of the boundary conditions as given in Table 1. Specifically, the Riemann and non-reflective boundary conditions serve to insure that the characteristic waves stay decoupled, which should mimic the scalar situation pretty closely. On the other hand, the use of reflective boundary conditions introduces wave reflections and interactions that are unique to the vector system.

The 4-frequency forcing function in Table 4 is selected as the baseline perturbation to obtain CFD solutions. The POD eigen-basis is generated based on the vector-valued method and the maximum values of each fluctuating quantities are used for normalization as mentioned in section A.

a. Effects of Mach number

The ROMs are generated based upon different conditions summarized in Table 3 from low to high Mach number. The ROM eigen-value spectrum for subsonic flow cases (A, B and C) is shown in Fig. 6 and it can be seen that for low Mach number (<0.5), unstable modes (highlighted in dashed circle) are still present while when the Mach number gets higher (>0.8), the resulting ROM becomes stable (negative real parts, σ). The reconstructed ROM solutions using the 4-frequency forcing function in Table 4 are compared against the CFD solutions for Case B and C in Fig. 7. As expected and similar to Fig. 5, unphysical amplitude growth that is markedly different from

the original CFD solution is seen for Case B, while a stable ROM is obtained for Case C, which correspondingly reproduces the original CFD solutions excellently.
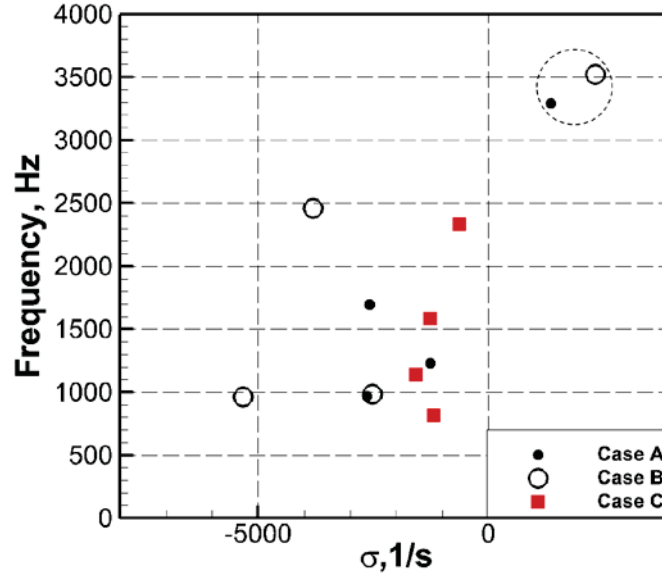

Figure 6 Eigen-value spectrum of ROM stiffness matrix for Case A, B and C (subsonic flow) in Table 3 using 4-frequency forcing function.

Case B   Case C
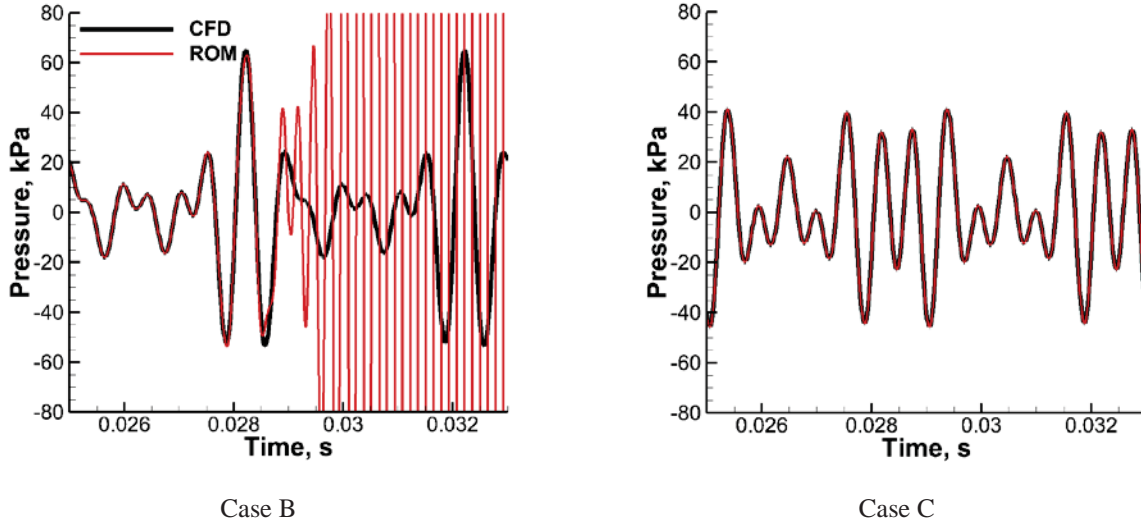
Figure 7 ROM and CFD solutions comparison at $x/L = 0.5$ for Case B (left) and C (right) in Table 3 using 4-frequency forcing.

As it goes to supersonic flow cases (D and E), all the resulting ROMs are stable based on the eigen-value spectrum shown in Fig. 8 with all the real parts of eigen-values being well below zero. The observations from Figs. 6 and 8 provide some clues as to the possible causes of the unstable eigen-modes in ROMs. As the Mach number of flow goes higher, the reflecting characteristic waves (or upstream traveling waves) from downstream boundary are

13

weakened and, when the flow becomes supersonic, there is no wave traveling back from the downstream end. This suggests that the ROM stability issues might be related to the simultaneous presence of downstream and upstream traveling waves in the CFD solution---a situation that only arises in the subsonic Euler system (and not in supersonic flow or in the scalar equation case). In turn, this motivates the study in the following section that studies the effects of boundary conditions which are also directly related to the wave characteristics of the CFD solution.
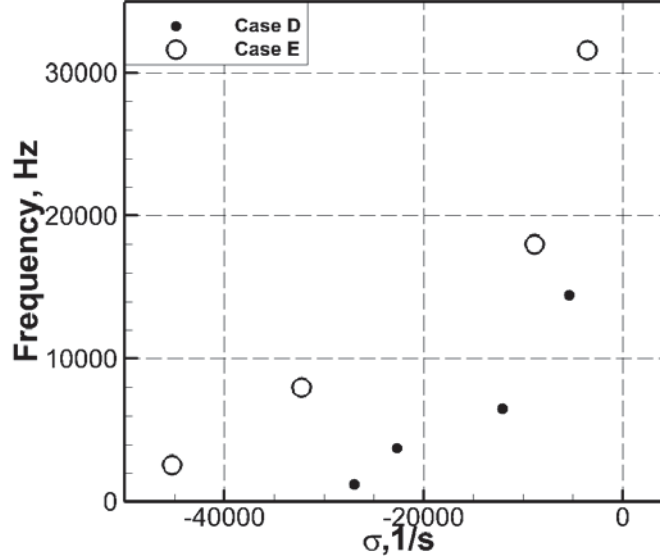

Figure 8 Eigen-value spectrum of ROM stiffness matrix for Case D and E (supersonic flow) in Table 3 using 4-frequency forcing function.

b. Effects of boundary conditions

Riemann invariant boundary conditions are implemented at both the upstream and downstream boundaries in order to eliminate wave reflections. The perturbations defined in Eq. (3) are applied for each of the characteristics waves individually using the 4-frequency forcing function in Table 4. By doing so, the downstream and upstream propagating waves are separated so that the waves do not interact. The Riemann variables correspond to propagating speeds, u, $u+c$ and $u-c$. Three cases are considered here: 1. only u and $u+c$ characteristic waves are perturbed while the downstream propagating wave ($u-c$) is kept unperturbed; 2. only u and $u-c$ characteristic waves are perturbed while the downstream propagating wave ($u+c$) is kept unperturbed; and 3. all characteristic waves are perturbed. The eigen-value spectrum of the resulting ROMs of these three cases are shown in Fig. 9. It can be readily seen that all ROMs are stable with negative real parts, σ, which confirms that as long as the waves are treated independent of each other, the Euler system reduces to a set of three scalar wave equations (at least in the linear limit) and the resulting ROM problem remains stable.
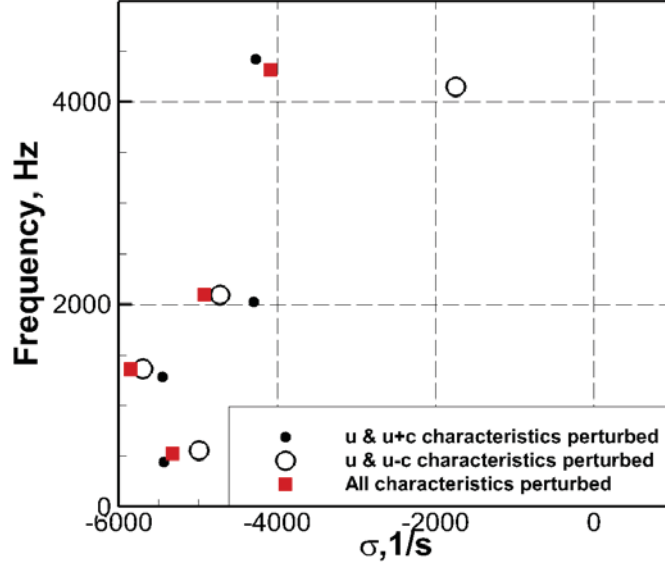
14

Figure 9 Eigen-value spectrum of ROM stiffness matrix for B.C. 2 in Table 1 using 4-frequency forcing function.

In the second instance, the mass flow rate is specified for upstream boundary (and forced), while a non-reflecting boundary condition is used downstream to eliminate wave reflections into the upstream propagating wave (u-c). The eigen-value spectrum of the resulting ROM for this case is shown in Fig. 10, which also does not show any unstable modes. This result should be contrasted with Case A in Fig. 6, which specified constant back pressure for the downstream boundary thereby allowing a reflected upstream-running characteristic wave. It can therefore be inferred that the boundary reflection of the upstream propagating wave (u-c) is a potential cause for the ROM stability issues.

Based on the results above, it can be concluded that the ROM stability issue arises when both considerable upstream and downstream propagating characteristics waves are present and mixed at the boundaries. Moreover, stable ROMs can be obtained in two major ways: (1) by reducing the upstream propagating wave by either increasing the flow Mach number or (2) by applying non-reflecting boundary conditions to avoid wave reflections. These findings clearly confirm why the stability issues occur in the vector Euler system case and not in the scalar equation studies. Of course, further study is needed to understand precisely why the ROM solutions are so influenced by the presence of boundary wave reflections and will be undertaken as part of future work. For now, we examine the possibility of mitigating the stability problems by the addition of artificial dissipation terms. This technique was originally proposed for ROM development using an incomplete POD eigen-bases, but we use it here for situations wherein a complete eigen-bases is used in the ROM construction.
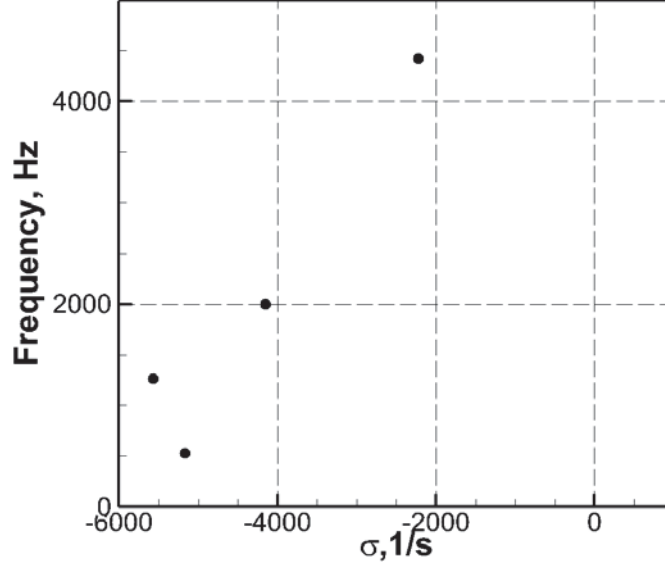
Figure 10 Eigen-value spectrum of ROM stiffness matrix for B.C. 3 in Table 1 using 4-frequency forcing function.

C. ROM stabilization through additional artificial dissipation

It has been shown in previous studies that a simple treatment like including additional artificial dissipation in building the ROM can useful to eliminate the non-physical unstable modes [15]. Here the method of including the artificial dissipation is briefly introduced starting with the discretized form of the linearized model equation, Eq. (2),

$$\overline{\Gamma}_{p,i}\frac{\partial Q'_{p,i}}{\partial t}\Delta x_i + \left(\overline{A}_p Q'_p\right)_{i+1/2} area_{i+1/2} - \left(\overline{A}_p Q'_p\right)_{i-1/2} area_{i-1/2} - \overline{D}_{p,i}Q'_{p,i}\Delta x_i = 0 \tag{12}$$

where Δx_i is the size of the ith cell and $area_{i+1/2}$ is the left/right faces area of the ith cell. The artificial dissipation is added at the cell faces,

$$\left(\overline{A}_p Q'_p\right)_{i+1/2} = \frac{1}{2}\left\{\left(\overline{A}_p Q'_p\right)^L_{i+1/2} + \left(\overline{A}_p Q'_p\right)^R_{i+1/2}\right\} - \frac{1}{2}\beta\underbrace{\left|\overline{A}_p\right|_{i+1/2}\left\{\left(Q'_p\right)^R_{i+1/2} - \left(Q'_p\right)^L_{i+1/2}\right\}}_{\text{Artificial Dissipations}}$$

$$\left(\overline{A}_p Q'_p\right)_{i-1/2} = \frac{1}{2}\left\{\left(\overline{A}_p Q'_p\right)^L_{i-1/2} + \left(\overline{A}_p Q'_p\right)^R_{i-1/2}\right\} - \frac{1}{2}\beta\underbrace{\left|\overline{A}_p\right|_{i-1/2}\left\{\left(Q'_p\right)^R_{i-1/2} - \left(Q'_p\right)^L_{i-1/2}\right\}}_{\text{Artificial Dissipations}} \tag{13}$$

It should be noted that the artificial dissipation already exists in the original CFD solutions since we are using a 2nd-order upwind discretization scheme (with $\beta = 1$), based upon which the POD eigen-basis is calculated. To increase the stabilizing influence of the ROM, different β values (>1) are used during the Galerkin projection step. By systematically varying the definition of the β parameter, we can estimate how much extra artificial dissipation is needed to stabilize the ROMs.
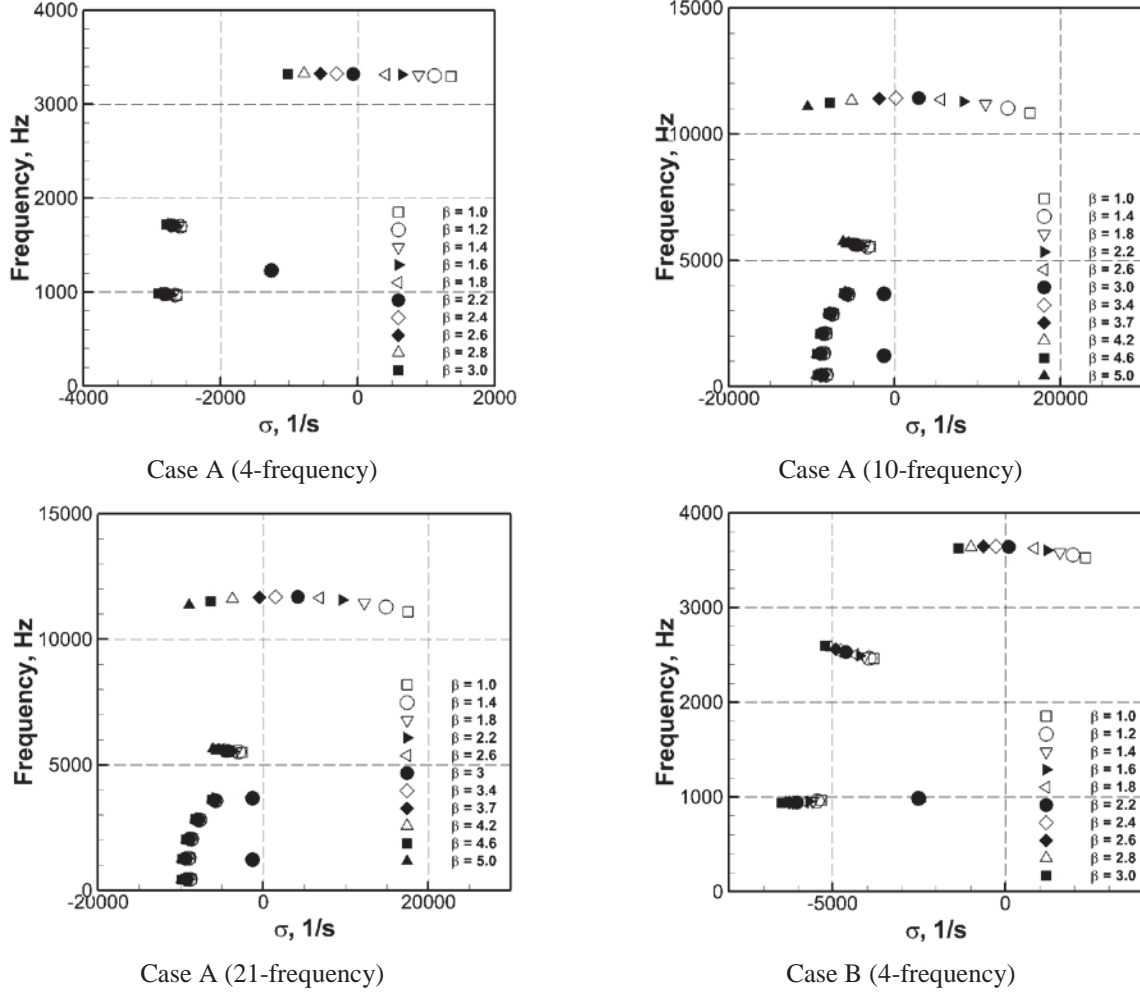
Figure 11 Eigen-value spectrum of ROM stiffness matrix by including different amounts of artificial dissipation

The four cases showing unstable modes in the resulting ROMs are selected from section A and B for further investigation. These are Case A (4-, 10- and 21-frequency) and Case B (4-frequency). The corresponding ROM eigen-value spectra are shown in Fig. 11 with different amounts of artificial dissipation added. It can be readily seen from the spectra that including additional dissipation (increasing the β value greater than unity) is able to stabilize the ROMs by reducing the real part (σ) of each mode while it does not materially affect the imaginary part (f) very much. Moreover, it is also observed to have a more significant effect on the unstable modes than on the stable modes, which is a desired property since we do not want to alter the physically accurate eigenmodes. For cases with less frequency diversity in the forcing function (4-frequency), the real part of the unstable mode is reduced below zero when β is increased up to 2.2 ~ 2.4, which means approximately twice the artificial dissipation is needed to generate a stable ROM. For cases with more frequency diversity in the forcing function (10- and 21-frequency), approximately 3 times more artificial dissipation is needed ($\beta \sim 3.7$) to stabilize the ROMs.
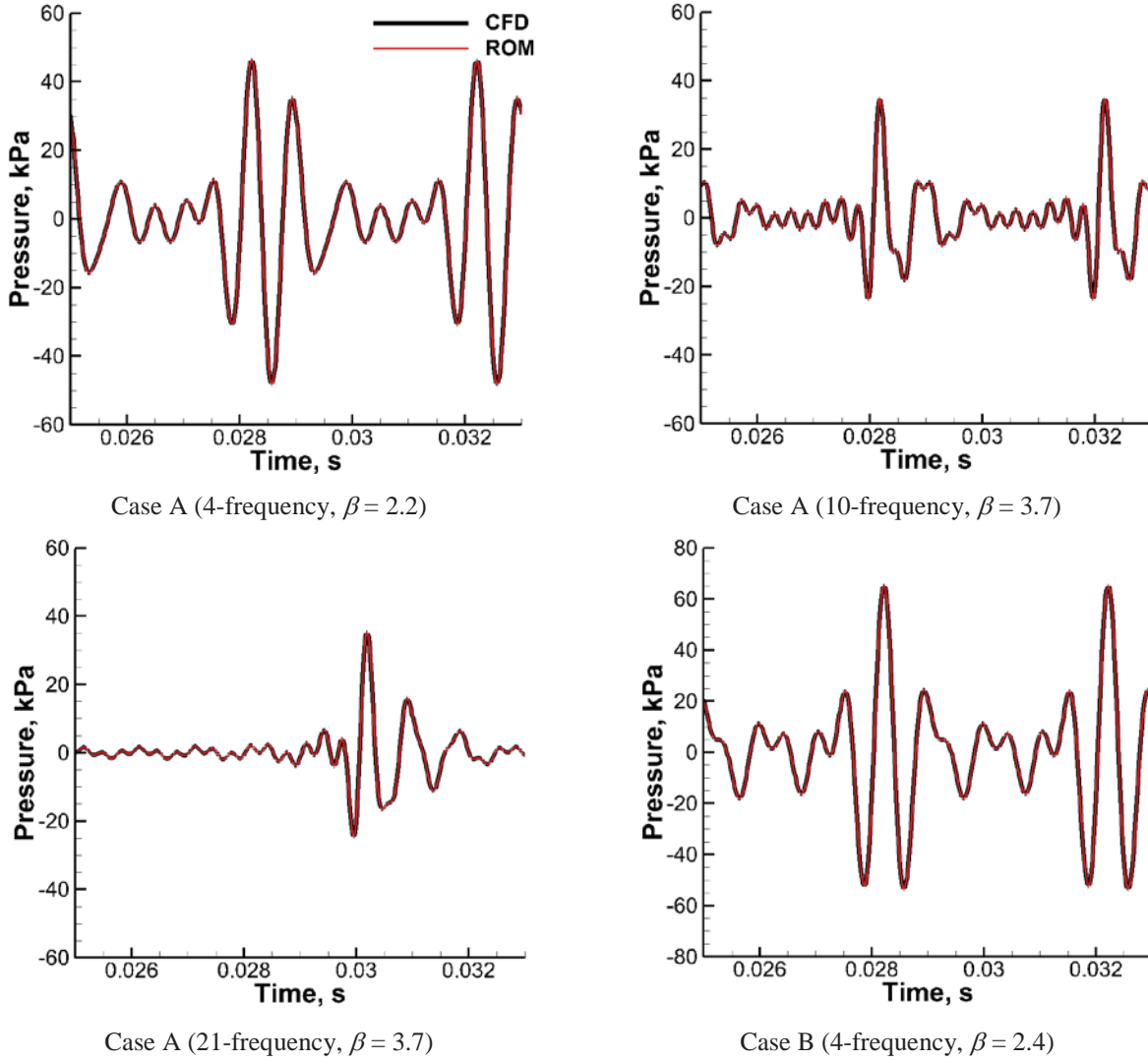
Figure 12 ROM and CFD solutions comparison at *x/L* = 0.5 by including additional artificial dissipations.

The stabilized ROMs with the corresponding β values are tested and validated against the CFD solutions in the same way as in Figs. 5 and 7. The reconstructed ROM solutions are shown in Fig. 12. All the stabilized ROMs are observed to predict solutions that are in excellent agreement with the CFD results. In contrast with the results in Figs. 5 (bottom) and 7, adding the additional amount of artificial dissipation is effective in dissipating the unphysical instabilities and enables the ROMs to capture the original CFD solutions very well.

VI. Conclusions

Stability issues encountered in previous studies using the POD/Galerkin method for reduced order model (ROM) development of the linearized Euler equations are investigated. For simplicity, the combustion response in our model equation is deactivated and only the gas dynamics are calculated to obtain the POD basis vector, which are then used within a Galerkin formulation to reduce the governing partial differential equations to a set of ordinary differential equations. Efforts have been made to resolve ROM stability issues by changing and scaling the solution variables used in POD mode generation, which shows some success but still does notguarantee a universally stable method. Hence, the studies in this paper are performed on two major aspects: first, to understand and identify possible causes of the non-physical instability issues present in the ROM development for vector systems of equations; second, to test and evaluate the addition of extra artificial dissipation to mitigate the ROM stability issues.

Even though only simple flow dynamics are solved, unstable modes are still encountered in the resulting ROMs and the inclusion of multiple frequencies in the forcing function appears to create more difficulties in obtaining a stable ROM. Different mean flow Mach numbers are tested to generate the ROMs and it is found that the ROM stability issues improve as the Mach number gets higher. Moreover, the system becomes completely stable for supersonic flows, which suggests that the reduction and eventual elimination of the upstream propagating characteristic waves is beneficial to stability. Following that, different boundary conditions are implemented to control the amount of upstream propagating waves present in the CFD solution. It has been shown that stable ROMs can be generated by applying either non-reflecting boundary condition downstream or Riemann invariant boundary conditions both upstream and downstream, which indicates the important role that the upstream traveling characteristic waves have on the overall ROM stability. A fundamental insight is that the elimination of wave reflections at boundaries essentially reduces the Euler equations to a system of independent characteristic waves that is equivalent to multiple scalar wave equations. Indeed, it is the interaction between waves that arises in the vector system that is at the source of the stability issues.

A simple solution is proposed to mitigate the instabilities by increasing the amount of artificial dissipation in the the Galerkin projection step. The additional dissipation is shown to have a more significant effect on the unstable modes, while they do not affect the stable modes very much. Thus, the stabilized ROMs prove to be able to reproduce the original CFD solutions with excellent agreement.

Overall, resolving stability issues identified in the ROM development for vector systems of equations remains an importantand highly challenging task. In the present paper, significant progress has been made to identify possible causes for spurious unstable modes in the ROM construction and the corresponding stabilization treatment. More detailed and systematic studies are needed to understand the underlying causes of the instability and to insure that the proposed addition of artificial dissipation remains robust for more complicated problems.

References

1.   Bergmann, M., Bruneau, C. H., and Iollo, A. "Enablers for robust POD models," *Journal of Computational Physics* Vol. 228, No. 2, 2009, pp. 516-538.

2.   Rowley, C. W. "Model Reduction for Fluids using Balanced Proper Orthogonal Decomposition," *International Journal of Bifurcation and Chaos*, 2005.

3.   Rowley, C. W., Colonius, T., and Murray, R. M. "Model reduction for compressible flows using POD and Galerkin projection," *Physica D: Nonlinear Phenomena* Vol. 189, No. 1-2, 2004, pp. 115-129.

4.   Barbagallo, A., Dergham, G., Sipp, D., Schmid, P. J., and Robinet, J.-C. "Closed-loop control of unsteadiness over a rounded backward-facing step," *Journal of Fluid Mechanics* Vol. 703, 2012, pp. 326-362.

5.   Barbagallo, A., Sipp, D., and Schmid, P. J. "Closed-loop control of an open cavity flow using reduced-order models," *Journal of Fluid Mechanics* Vol. 641, 2009, p. 1.

6.   Barbagallo, A., Sipp, D., and Schmid, P. J. "Input–output measures for model reduction and closed-loop control: application to global modes," *Journal of Fluid Mechanics* Vol. 685, 2011, pp. 23-53.

7.   Lieu, T., and Farhat, C. "Adaptation of Aeroelastic Reduced-Order Models and Application to an F-16 Configuration," *AIAA Journal* Vol. 45, No. 6, 2007, pp. 1244-1257.

8.   Lucia, D. J., Beran, P. S., and Silva, W. A. "Reduced-order modeling: new approaches for computational physics," *Progress in Aerospace Sciences* Vol. 40, No. 1-2, 2004, pp. 51-117.

9.   Munipalli, R., Zhu, X., Menon, S., and Hesthaven, J. "Model Reduction Opportunities in Detailed Simulations of Combustion Dynamics," *52nd Aerospace Sciences Meeting*. National Harbor, Maryland, 2014.

10.   Huang, X., and Baumann, W. T. "Reduced-Order Modeling of Dynamic Heat Release for Thermoacoustic Instability Prediction," *Combustion Science and Technology* Vol. 179, No. 3, 2007, pp. 617-636.

11.   Huang, C., Anderson, W. E., Merkle, C., and Sankaran, V. "Exploration of POD-Galerkin Method in Developing a Flame Model for Combustion Instability Problems," *7th AIAA Theoretical Fluid Mechanics Conference*. Atlanta, GA, 2014.

12.   Rempfer, D. "On Low-Dimensional Galerkin Models for Fluid Flow," *Theoretical and Computational Fluid Dynamics* Vol. 14, 2000, pp. 75–88.

13.   Noack, B. R., Papas, P., and Monkewitz, P. A. "The need for a pressure-term representation in empirical Galerkin models of incompressible shear flows," *Journal of Fluid Mechanics* Vol. 523, 2005, pp. 339-365.

14.   Willcox, K., and Peraire, J. "Balanced Model Reduction via the Proper Orthogonal Decomposition," *AIAA Journal* Vol. 40, 2002.

15.   Lucia, D. J., and Beran, P. S. "Projection methods for reduced order models of compressible flows," *Journal of Computational Physics* Vol. 188, No. 1, 2003, pp. 252-280.

16.   Huang, C., Anderson, W. E., Merkle, C., and Sankaran, V. "Exploration of POD-Galerkin Techniques for Developing Reduced Order Models of the Euler Equations," *51st AIAA/SAE/ASEE Joint Propulsion Conference*. Orlando, FL, 2015.

17. Barone, M., Segalman, D., Thornquist, H., and Kalashnikova, I. "Galerkin Reduced Order Models for Compressible Flow with Structural Interaction," *46th AIAA Aerospace Sciences Meeting and Exhibit*. Reno, Nevada, 2008.

18. Barone, M. F., Kalashnikova, I., Brake, M. R., and Segalman, D. J. "Reduced Order Modeling of Fluid/Structure Interaction." Sandia National Laboratories, 2009.

19. Amsallem, D., and Farhat, C. "On the Stability of Linearized Reduced-Order Models: Descriptor vs. Non-Descriptor Form and Application to Fluid-Structure Interaction," *42nd AIAA Fluid Dynamics Conference and Exhibit*. New Orleans, Louisiana, 2012.

20. Crocco, L., Grey, J., and Harrjet, D. T. "On the Importance of Sensitivity Time Lag in Longitudinal High-frequency Rocket Combustion Instability," *Jet Propulsion* Vol. 28, No. 12, 1958, pp. 841-843.

21. Smith, R. J., Xia, G., Sankaran, V., Anderson, W. E., and Merkle, C. L. "Computational Investigation of Acoustics and Instabilities in a Longitudinal Mode Rocket Combustor," *AIAA Journal* Vol. 46, 2008.